



Microcombustion for micro-tubular flame-assisted fuel cell power and heat cogeneration

Ryan J. Milcarek^{a,*}, Hisashi Nakamura^b, Takuya Tezuka^b, Kaoru Maruta^b, Jeongmin Ahn^c

^a School for Engineering of Matter, Transport and Energy, Arizona State University, 501 E. Tyler Mall, Tempe, AZ, 85287, USA

^b Institute of Fluid Science, Tohoku University, 2-1-1 Katahira, Aoba, Sendai, 980-8577, Japan

^c Department of Mechanical and Aerospace Engineering, Syracuse University, Syracuse, NY, 13244, USA

HIGHLIGHTS

- A non-catalytic concept for microcombustion based flame-assisted fuel cells.
- Gas phase reactions at high equivalence ratios visualized with experimental setup.
- Soot formation avoided at high equivalence ratios (> 5) and low temperature (< 900 °C).
- Micro-tubular flame-assisted fuel cells achieve over 50% fuel utilization.
- Significant power density of $\sim 450 \text{ mW cm}^{-2}$ is achieved in combustion exhaust.

ARTICLE INFO

Keywords:

Flame-assisted fuel cell (FFC)
Solid oxide fuel cell (SOFC)
Micro flow reactor
Microcombustion
Micro heat and power cogeneration

ABSTRACT

Flame-assisted fuel cell (FFC) studies have been limited to lower fuel-rich equivalence ratios (~ 1 – 1.7 , due to the upper flammability limit and sooting limit) where only small concentrations of H_2 and CO can be generated in the exhaust. In this work, a non-catalytic microcombustion based FFC is proposed for direct use of hydrocarbons for power generation. The potential for high FFC performance (450 mW cm^{-2} power density and 50% fuel utilization) in propane/air microcombustion exhaust is demonstrated. The micro flow reactor is investigated as a fuel reformer for equivalence ratios from 1 to 5.5. One significant result is that soot formation in the micro flow reactor is not observed at equivalence ratios from 1 to 5.5 and maximum wall temperatures ranging from 750 to 900 °C. Soot formation is observed at higher wall temperatures of 950 °C and 1000 °C and equivalence ratios above 2.5. H_2 and CO concentrations in the exhaust are found to have a strong temperature dependence that varies with the maximum wall temperature and the local flame temperature.

1. Introduction

Direct Flame Fuel Cells (DFFCs) are Solid Oxide Fuel Cells (SOFCs) which are placed directly in a flame in a ‘no chamber’ setup for direct conversion of syngas to electrical power [1–10]. The setup is characterized by premixed fuel and air at a specified equivalence ratio, which is ignited in the ambient for partially premixed combustion. The SOFC is brought to operating temperature (500–1000 °C) by being placed directly in the flame where syngas and other unburned hydrocarbons are present. Challenges in DFFC research include low electrical efficiency ($< 0.5\%$) [4,7] and low power density (often below 400 mW cm^{-2}) [10]. Recently a Flame-assisted Fuel cell (FFC) was proposed, which is like a DFFC, but operates in a dual-chamber configuration [11,12] with a combustion chamber upstream of the SOFC

[13–18]. This premixed combustion system avoids complete oxidation of the fuel with excess air which is present in conventional DFFCs. As a result, more fuel enters the SOFC anode for electrochemical power generation which is expected to yield higher electrical efficiency and power density [15]. The fuel/air equivalence ratio is a dominant factor in these studies as the highest syngas concentration occurs at higher equivalence ratios. However, the upper flammability limit [19] has limited the highest attainable syngas generation to only 12.4% H_2 and 8.7% CO in methane combustion exhaust at an equivalence ratio of 1.4 [13] and 12.7% H_2 and 12.3% CO in propane combustion exhaust at an equivalence ratio of 1.7 [20].

One approach to overcoming the flammability limit is to utilize catalytic reforming of hydrocarbons instead of the gas phase combustion reactions in DFFCs and FFCs. This approach has been investigated

* Corresponding author.

E-mail address: Ryan.Milcarek@asu.edu (R.J. Milcarek).

<https://doi.org/10.1016/j.jpowsour.2018.12.043>

Received 17 October 2018; Received in revised form 3 December 2018; Accepted 17 December 2018

0378-7753/ © 2018 Elsevier B.V. All rights reserved.

extensively since the late 1990s with a catalytic tube reformer and tubular SOFC [21–23]. It has since been commercialized.

Another option for overcoming the upper flammability limit without the use of a catalyst is to utilize superadiabatic combustion. While the upper flammability limit is an issue in conventional burners, in superadiabatic combustion [24], which utilizes heat recirculation, the notion of an upper flammability limit is less relevant [25,26]. Heat recirculation to preheat the fuel/air mixture can prevent quenching and allow self-sustained reactions in the ultra-rich and ultra-lean regimes [26]. The micro flow reactor with controlled temperature profile [27,28], parallel channel reactor [26,29], porous media reactor [30,31], swiss roll reactor [32,33] and spouted bed reactor [34] have been investigated with heat recirculation. Large syngas concentrations in the exhaust exceeding 30% have been reported in the ultra-rich regime at equivalence ratios around 2.5 in many of these studies.

While fuel-rich equivalence ratios exceeding the upper flammability limit are possible with heat recirculation, soot formation is a concern. Soot formation is often documented with the lowest equivalence ratio at which soot formation can be observed and it is often in the range 1.1–1.8 for many fuels [35]. Most DFFC studies have been conducted below this limit, but maximum syngas formation often occurs at higher equivalence ratios. The critical equivalence ratio for soot formation has a strong temperature dependence with the critical equivalence ratio observed to increase with temperature (above $1127^\circ\text{C} = 1400\text{ K}$) [35]. Few studies at temperatures below 1127°C exist. The micro flow reactor with controlled temperature profile has provided a novel means of studying flame characteristics at lower temperatures and recent studies have suggested that the critical sooting limit may be higher (i.e., less sooting) at temperatures below 1127°C [36,37]. In one case, no soot formation was observed when the wall temperature of the micro flow reactor did not exceed 827°C , even at an equivalence ratio of 4 with n-cetane and iso-cetane fuel [37]. Therefore, the micro flow reactor may provide a means of fuel reformation at high equivalence ratios (> 3 , by utilizing heat recirculation) without any soot formation (by limiting the maximum wall temperature). The use of the micro flow reactor for fuel reforming at high equivalence ratios and low temperatures needs investigation.

In this work, a non-catalytic micro flow reactor and micro-Tubular FFC (mT-FFC) micro heat and power cogeneration setup is discussed. A micro tubular SOFC [38] is sealed directly to the end of the micro flow reactor with controlled temperature profile [27] providing a micro-combustion based fuel reformation of hydrocarbons followed by direct utilization of the syngas and smaller hydrocarbons in the mT-FFC. Remaining fuel is combusted and heat can be recovered for various applications.

2. Experimental setup

2.1. Fuel cell fabrication and characterization

The micro tubular SOFC anode ($\text{Ni} + (\text{Y}_2\text{O}_3)_{0.08}(\text{ZrO}_2)_{0.92}$ (YSZ)) and electrolyte (YSZ) were fabricated as previously reported [13,15]. The inside diameter of the anode was 2.4 mm and the outside diameter was 3.3 mm. In order to investigate temperatures below 827°C , a $\text{Sm}_{0.20}\text{Ce}_{0.80}\text{O}_{2-x}$ (SDC) buffer layer [11,12] was applied to the YSZ electrolyte using a wet powder spray technique, dried and sintered at 1350°C for 4 h. A $(\text{La}_{0.60}\text{Sr}_{0.40})_{0.95}\text{Co}_{0.20}\text{Fe}_{0.80}\text{O}_{3-x}$ (LSCF) + SDC (7:3 w/w) cathode was dip coated onto the SDC buffer layer, dried and sintered to 1100°C for 4 h. Silver paste was used for cathode current collection with an active area of 1.66 cm^2 . The SOFC was sealed to the end of a quartz tube (3.6 mm ID), hereafter referred to as the micro flow reactor, using ceramic paste. Testing of the micro tubular SOFC occurred at two temperatures (750°C and 800°C) in a horizontal split tube furnace. The current-voltage method with four probe technique was utilized for electrochemical characterization of the SOFC. A Keithley 2420 sourcemeter was interfaced with a computer and mass

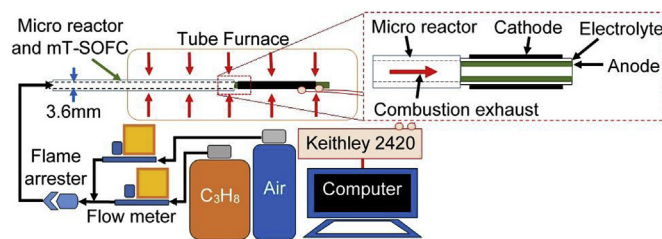


Fig. 1. mT-FFC characterization setup.

flow controllers were controlled with LabVIEW software. Propane was used as the fuel in this study. The flow rate of propane was fixed during testing and the air flow rate was adjusted to achieve the proper equivalence ratio. Equivalence ratio (Φ) is defined in Eq. (1) where n_{fuel} and n_{air} denote the molar flow rates of fuel and air, respectively; and n_{fuel}^S and n_{air}^S denote the molar flow rates required for stoichiometric combustion of fuel and air, respectively. K-type thermocouples monitored the temperature of the inside of the micro flow reactor, hereafter referred to as the wall temperature, and the SOFC anode temperature. Fig. 1 shows the experimental setup.

$$\Phi = \frac{n_{\text{fuel}}/n_{\text{air}}}{n_{\text{fuel}}^S/n_{\text{air}}^S} \quad (1)$$

2.2. Microcombustion characterization

Characterization of the microcombustion of propane/air was conducted in the same micro flow reactor with a previously reported flat flame burner setup for flame visualization [36,37]. The micro flow reactor utilized in both the fuel cell and microcombustion characterization experiments has the following characteristics. The fuel/air mixture is sent to the micro flow reactor at ambient temperature. Upon entering the furnace or passing through the flat flame burner, the wall temperature rises until it reaches a maximum value which was carefully controlled in these experiments. The flame stabilizes in the region of maximum wall temperature for both experiments. The maximum wall temperature at the bottom inner surface of the micro flow reactor was measured with a K-type thermocouple. An example of a typical wall temperature profile for a maximum wall temperature of 750°C is shown in Fig. A.1 in the appendix. Further details on the micro flow reactor with controlled temperature profile can be found in the authors previous work [33,34]. Two types of experiments were performed for the microcombustion characterization. First, the flame and sooting characteristics of propane/air microcombustion were investigated for equivalence ratios from 1 to 5.5, total flow rates from 10 to 180 mL min^{-1} (velocities from 1.6 to 30 cm s^{-1}), and temperatures of $750, 800, 850, 900, 950$ and 1000°C . A digital camera (Nikon D300S) was used to take images of the flame and thermal radiation from the soot in the reactor. The flow rate of fuel and air were set to the proper equivalence ratio and the flame stabilized for 40s before taking an image. A regime map of flame and soot characteristics was plotted on the flow rate vs. equivalence ratio plane. A second set of experiments investigated the microcombustion exhaust composition for a fixed propane flow rate of 2 mL min^{-1} with equivalence ratios from 1 to 5.5 and maximum wall temperatures of $750, 800, 850, 900, 950$ and 1000°C . Exhaust gas was sampled with a gas chromatograph (GC-2010 Plus) with a BID-2010 Plus detector. As an example of the equivalence ratio calculations and the flow rates utilized, Table 1 shows flow rates for the experiments with a fixed propane flow rates of 2 mL min^{-1} .

Table 1Propane/air flow rates for different equivalence ratios and a fixed propane flow rate of 2 mL min^{-1}

Equivalence ratio, Φ	Propane flow rate (mL min^{-1})	Air flow rate (mL min^{-1})
1.4	2	34.00
1.6	2	29.75
1.8	2	26.44
2.0	2	23.80
2.2	2	21.64
2.4	2	19.83
2.6	2	18.31
2.8	2	17.00
3.0	2	15.87
3.2	2	14.88
3.4	2	14.00
3.6	2	13.22
3.8	2	12.53
4.0	2	11.90
4.2	2	11.33
4.4	2	10.82
4.6	2	10.35
4.8	2	9.92
5.0	2	9.52
5.2	2	9.15

3. Results

3.1. Microcombustion reforming characterization

Fig. 2 shows the microcombustion flame characteristics at wall temperatures of 900°C and 1000°C . The Flame with Repetitive Extinction and Ignition (FREI) regime for this 3.6 mm micro flow reactor with controlled temperature profile was observed at stoichiometry for mixture flow rates between 10 and 140 mL min^{-1} (velocities between 1.6 and 23 cm s^{-1}), which is similar to previously reported work on a 2 mm micro flow reactor with controlled temperature profile [27]. The velocity range over which the FREI existed narrowed as the equivalence ratio increased, as observed in other work [39], to the point where no FREI regime was observed at an equivalence ratio of 2.5 . The main observation from Fig. 2a is that at a wall temperature of 900°C , no soot was observed at any velocity even at an equivalence ratio of 5.5 . No soot formation was observed at an equivalence ratio of 5.5 with a wall temperature of 750 , 800 or 850°C at any of the flow rates investigated in this work. The regime maps at these lower temperatures were similar to the regime map at 900°C (Fig. 2a), and are not repeated. Similar regimes for the normal flame, FREI and weak flame were observed when the wall temperature was increased to 1000°C . However, radiation from soot was observed above an equivalence ratio of 2.5 as shown

in Fig. 2b. Further investigation revealed that the sooting characteristics at 950°C were the same as shown in Fig. 2b at 1000°C . Representative direct images of the propane/air flame and soot responses for a fixed total flow rate of 100 mL min^{-1} are shown in Fig. 3 for equivalence ratios (Φ) from 1 to 5 and maximum wall temperatures of 900 and 1000°C . The results shown in Figs. 2 and 3 indicate that if the micro flow reactors wall temperature is in the range of 750 – 900°C soot formation does not occur for equivalence ratios 1 – 5.5 under the experimental procedure used here, providing a wide operating range for the mT-FFC.

With no soot observed for equivalence ratios 1 – 5.5 at wall temperatures in the range of 750 – 900°C , the microcombustion exhaust of propane/air was investigated at 750 , 800 , 850 and 900°C . Fig. 4 shows the results for a fixed propane flow rate of 2 mL min^{-1} . As shown in Fig. 4a, the H_2 in the exhaust remained just below 3.6 mol\% at a wall temperature of 750°C . The H_2 concentration increased quickly below an equivalence ratio of 2 , but was fairly stable at higher equivalence ratios. The CO concentration showed a similar trend, but the concentration remained between 9.8 and 10.7 mol\% above an equivalence ratio of 2 . Other hydrocarbons were also observed throughout the range and increased with equivalence ratio. Increasing the wall temperature has a significant impact on the exhaust composition as shown by comparing Fig. 4a–d. As the wall temperature increased, the exhaust composition indicates a transition from incomplete combustion with CO , CH_4 , C_2H_4 and C_2H_6 as the 4 major species besides N_2 , toward smaller hydrocarbons with major species of H_2 , CO , CH_4 and C_2H_2 . This is expected as the propane oxidation mechanism proceeds from C_2H_6 to C_2H_4 and finally to C_2H_2 [40]. At higher equivalence ratios the presence of C_2 species results from propane breaking down to smaller hydrocarbons. The reactions proceed towards syngas, carbon dioxide, water and methane, which are the main byproducts expected from chemical equilibrium of propane/air under fuel-rich conditions [20]. A peak H_2 concentration of 9.2 mol\% and CO concentration of 15.3 mol\% occurred at an equivalence ratio of 3 with a wall temperature of 900°C as shown in Fig. 4d. The exhaust composition for a wall temperature of 950°C and 1000°C were investigated in the non-sooting region for equivalence ratios from 1 to 2.5 . The composition of the syngas in the exhaust at 950°C and 1000°C was comparable to the results at 900°C , was within experimental uncertainty and is therefore not shown here.

Increasing the wall temperature has a significant effect on the exhaust composition as just described. The local flame temperature can also be increased by increasing the flow rate, as observed in previous work [30,31]. To investigate the effect of local flame temperature the propane flow rate was increased from 2 to 6 mL min^{-1} and held constant while varying the equivalence ratio. Fig. 5 shows a comparison of the H_2 , CO and CH_4 concentration in the exhaust at fixed propane flow

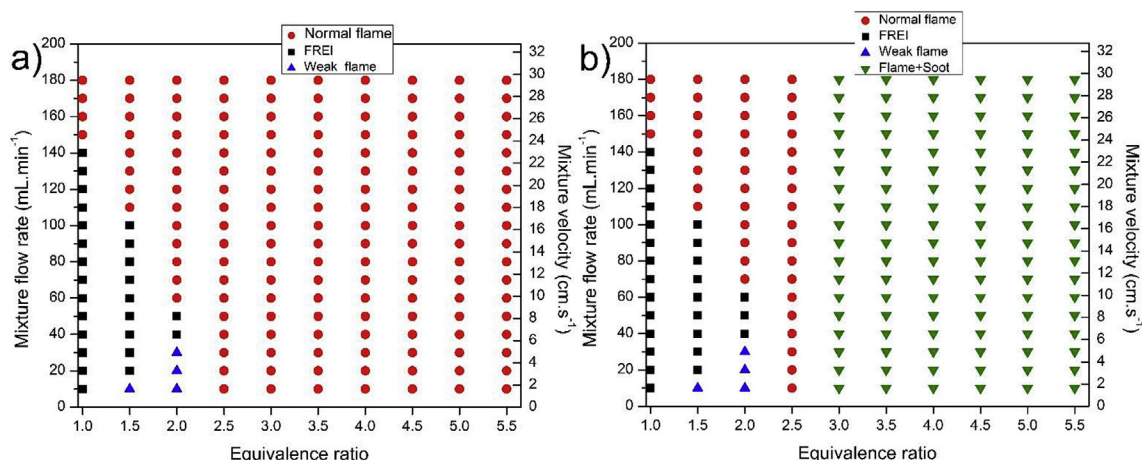


Fig. 2. Regime map showing weak flame, FREI, normal flame and flame with soot formation regions for propane/air microcombustion at a) 900°C and b) 1000°C .



Fig. 3. Representative direct image of propane/air flame and soot responses with fixed 100 mL min^{-1} total flow rate at 900°C and 1000°C and equivalence ratios from 1 to 5.

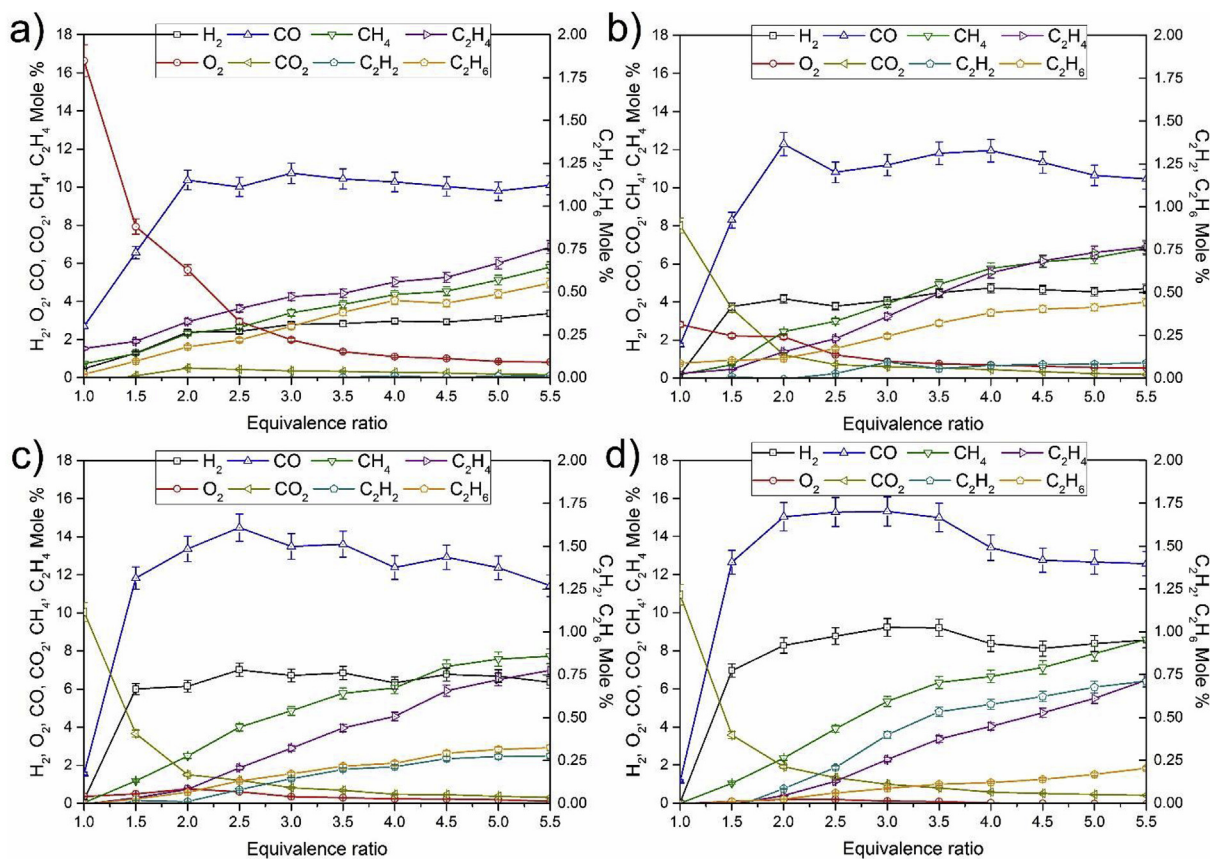


Fig. 4. Propane/air microcombustion exhaust species at equivalence ratios 1–5.5 and maximum wall temperature of a) 750°C , b) 800°C , c) 850°C and d) 900°C .

rates of 2 and 6 mL min^{-1} at a wall temperature of 800°C . The impact of increasing the flow rate on the syngas concentration was significant as the H_2 concentration increased from $4.2 \text{ mol}\%$ to $10.9 \text{ mol}\%$ and the CO concentration from $12.4 \text{ mol}\%$ to $14.7 \text{ mol}\%$ at an equivalence ratio of 2. A corresponding decrease in the higher hydrocarbons occurred as the flow rate increased.

3.2. Flame-assisted fuel cell performance

After characterizing the microcombustion exhaust composition the mT-FFC was tested at 800°C with a fixed propane flow rate of 2 mL min^{-1} and equivalence ratios ranging from 1.4 to 5.2. Fig. 6 shows the polarization and power density curves. To improve the clarity of Fig. 6 only the polarization and power density curves for equivalence ratios of 1.4, 1.8, 2.2, 2.6, 3.0, 3.4, 3.8, 4.2, 4.6, 5.0 and 5.2 are shown. Fig. 6a shows a significant (56%) increase in power density from a maximum power density of 220 mW cm^{-2} at an equivalence ratio of 1.4 up to 343 mW cm^{-2} at an equivalence ratio of 2. This occurred despite only increasing the incoming fuel concentration by 28% between an equivalence ratio of 1.4 and 2. The source of

this drastic increase in power density as the equivalence ratio increases is attributed to the increase in H_2 and CO concentrations, as shown in Fig. 4b. The power density increased further up to a peak of 460 mW cm^{-2} at an equivalence ratio of 4.6. Overall, the power density increased 109% as the equivalence ratio increased from 1.4 to 4.6. However, more than half of the increase occurred between an equivalence ratio of 1.4 and 2. Fig. 6b shows a much smaller and slower increase in power density between an equivalence ratio of 3.4 and 4.6. Beyond the optimal power density at an equivalence ratio of 4.6, the power density began to decline and there was evidence of carbon coking in the mT-FFC. Investigation of the exhaust species in Fig. 4b indicate that the CO concentration was decreasing above an equivalence ratio of 4.6 while the H_2 concentration was essentially constant. The presence of CH_4 , C_2H_2 , C_2H_4 and C_2H_6 are likely responsible for the carbon coking observed which can be mitigated by operating at lower equivalence ratios. Despite the carbon coking, the mT-FFC was able to achieve a high power density on this initial test without optimization of the microcombustion exhaust or fuel cell providing motivation for further investigation.

After observing an optimal equivalence ratio, beyond which carbon

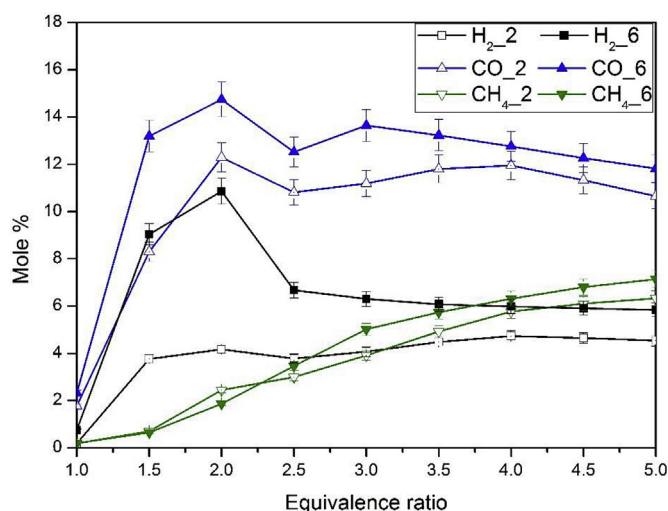


Fig. 5. Propane/air microcombustion exhaust comparison of H₂, CO and CH₄ at equivalence ratios 1–5 at fixed propane flow rate of 2 mL min⁻¹ and 6 mL min⁻¹.

deposition became apparent at 800 °C, the mT-FFC was investigated at 750 °C. The results are not repeated here as they are similar to the results shown in Fig. 6. The power density decreased slightly as expected due to the decrease in electrode kinetics with decreasing temperature and reduced H₂ and CO concentration (shown in Fig. 4a). However, the optimal power density of 337 mW cm⁻² occurred at an equivalence ratio of 3.2. The effect of carbon deposition became apparent at much lower equivalence ratios which could be due to some deterioration in the electrode, which occurred during testing at 800 °C and high equivalence ratios, but could also be due to a reduction in H₂ concentration. Fig. 7 provides a comparison of the fuel utilization of the two tests. This fuel utilization calculation is based on a previously reported method for mT-FFCs [7]. The fuel utilization accounts for the amount of fuel actually utilized (i.e., fuel remaining after microcombustion) in the electrochemical reactions compared to the initial fuel available (i.e., incoming propane). The fuel utilization can be defined by Eq. (2).

$$\varepsilon_{F.U.} = \frac{\text{Fuel consumed in SOFC}}{\text{Total fuel available before microcombustion}} \quad (2)$$

The fuel utilization can be calculated with Eq. (3)

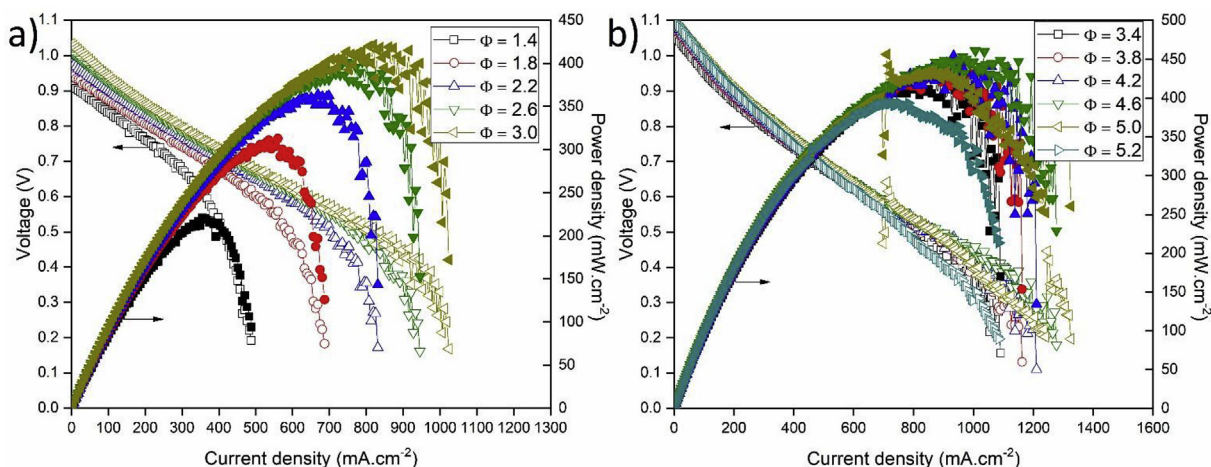


Fig. 6. mT-FFC polarization and power density at fixed propane flow rate of 2 mL min⁻¹, 800 °C and equivalence ratios from a) 1.4–3.2 and b) 3.4–5.2.

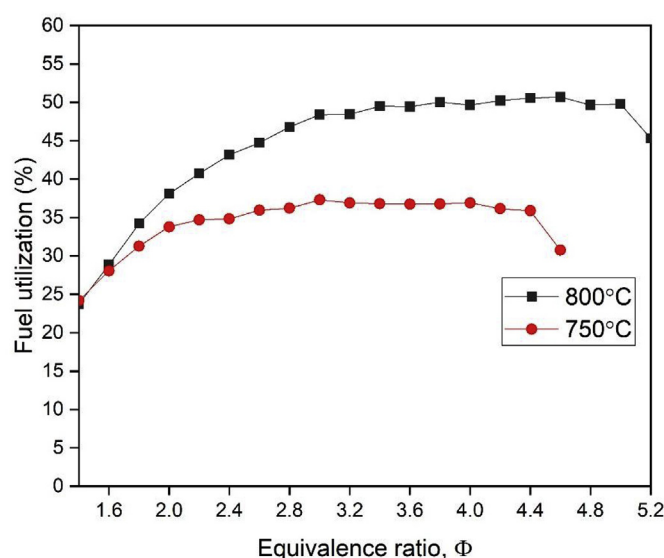


Fig. 7. mT-FFC fuel utilization at fixed propane flow rate of 2 mL min⁻¹, equivalence ratios from 1.4 to 5.2, a fuel cell operating voltage of 0.5 V and temperature of 750 °C and 800 °C.

$$\varepsilon_{F.U.} = \frac{i}{\frac{V_{fuel}}{V_M} \frac{1 \times 10^{-6}}{60} nF} \quad (3)$$

In Eq. (3), i [A] is the current being drawn from the SOFC at 0.5 V, V_{fuel} [mL.min⁻¹] is the total flow rate of propane, V_M [m³ mol⁻¹] is the molar volume at standard conditions, which is 2.24×10^{-2} m³ mol⁻¹, n is the moles of electrons per moles of fuel (i.e., 20 for propane) and F is Faradays constant. There are also numerical constants in Eq. (3) for unit conversion. The potential for high fuel utilization from this microcombustion mT-FFC power generation concept is evident by the peak fuel utilization of 50.7% at 800 °C and 0.5 V. For microcombustion based power generation, electrical efficiency often does not exceed 4% in heat engines [41,42]. Optimization of the mT-FFC microstructure and microcombustion exhaust species, a larger active area, and a well-designed heat recovery system may allow for high fuel utilization and electrical efficiency for this concept.

A final test on the mT-FFC was conducted to investigate the impact of changes in flow rate on the mT-FFC performance at a fixed equivalence ratio. Fig. 8a shows the change in fuel cell performance at different propane flow rates of 2, 3, 4, 5, and 6 mL min⁻¹ and a fixed equivalence ratio of 1.4. Similar results are shown for a fixed equivalence ratio of 2.5 in Fig. 8b. Both results showed an increase in power

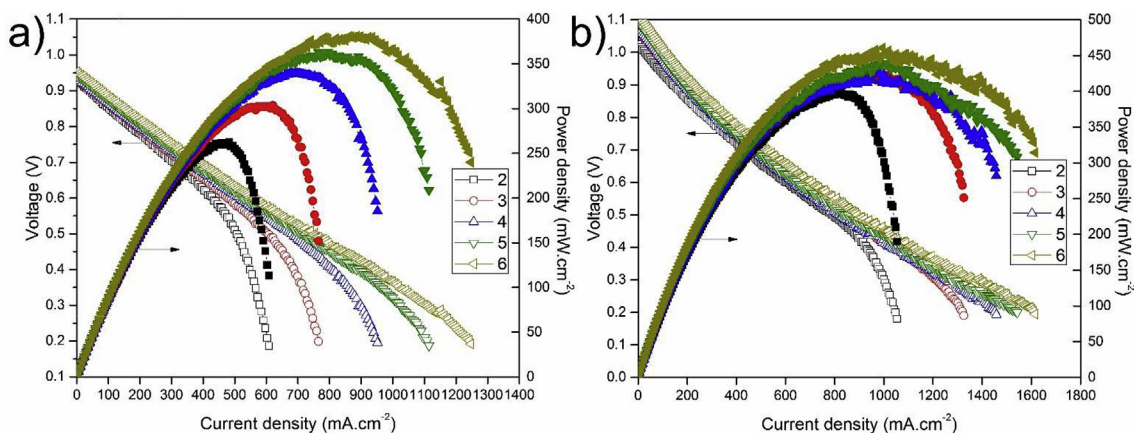


Fig. 8. mT-FFC polarization and power density at fixed propane flow rates of 2, 3, 4, 5 and 6 mL min^{−1} and equivalence ratios of a) 1.4 and b) 2.5.

density as the flow rate increased. While increasing the flow rate generally provides an increase in SOFC power density due to more fuel available for the fuel cell, there is a distinction between Fig. 8a and b. Fig. 8a shows a 45% increase in peak power density by increasing the propane flow rate from 2 to 6 mL min^{−1} at an equivalence ratio of 1.4. In comparison the peak power density increased by less than 16% at an equivalence ratio of 2.5. The reason for the significant difference in power density increase at these two equivalence ratios can be explained with the data shown in Fig. 5. The significant increase in H₂ (140% increase) and CO (59% increase) (Fig. 5) at an equivalence ratio of 1.5 helps explain the significant change in mT-FFC peak power density observed in Fig. 8a. H₂ kinetics in the anode are 2–3 times faster than CO kinetics [43] and certainly much faster than hydrocarbon kinetics which explains the steep increase in performance at an equivalence ratio of 1.5. In comparison, the increase in H₂ (76% increase) and CO (25% increase) was less significant at an equivalence ratio of 2.5 (Fig. 5), and the presence of higher hydrocarbons can slow the reactions which explains the results in Fig. 8b.

After operating in propane microcombustion exhaust (i.e., premixed fuel/air are fed to the micro flow reactor and the exhaust passes to the anode of the mT-FFC), the fuel was switched to propane only (i.e., no air was supplied for microcombustion to occur in the micro flow reactor) at flow rates of 2, 3, 4, 5 and 6 mL min^{−1}. A comparison of the mT-FFC performance in propane and propane microcombustion exhaust was sought, but the fuel cell cracked within 5 min after using pure propane at a flow rate of 4 mL min^{−1} due to rapid carbon deposition on the anode. This result was confirmed in multiple tests with a new SOFC indicating that the carbon deposition was not a result of the previous testing in microcombustion exhaust. Direct use of propane is ideal, but not possible due to rapid carbon deposition. However, testing in microcombustion exhaust was sustained for more than 5 h during the testing described here without any cracking of the fuel cell observed.

From this initial work, it is evident that the syngas concentration in the exhaust is temperature dependent and can be optimized with changes to the wall temperature and flow rate. Long term stable performance of a microcombustion based mT-FFC at high equivalence ratios is possible without soot formation as demonstrated, but the presence of CH₄, C₂H₂, C₂H₄ and C₂H₆ will need further investigation. Long-term, direct use of the C₂ species will either require a change in anode material or use of the water gas shift reaction to prevent carbon deposition on the anode. For example, Ni + YSZ can be replaced with a Cu-ceria anode, because Cu is a poor catalyst for C–H bond activation and graphite formation [44,45]. Ceria has high activity for hydrocarbon oxidation, high ionic conductivity and stable operation with methane, ethane, butane, 1-butene, and toluene has been achieved with no carbon deposition [44]. Alternatively, if the wall temperature and flow rate are optimized to limit the concentration of the hydrocarbons then

steam reforming on the Ni + YSZ anode is possible because of the presence of water in the exhaust. In one study with 1000 ppm of C₂H₄ and 3 mol% water at 800 °C, no carbon deposition was observed due to steam reforming on Ni + YSZ [46]. Equation (4) shows an example for CH₄ steam reforming.



4. Conclusions

In this work, an upstream quartz tube has been used to study controlled propane microcombustion over equivalence ratios ranging from 1 to 5.5 and temperatures ranging from 750 °C to 1000 °C. The mT-FFC downstream of the microcombustion was monitored. Microcombustion was observed through the quartz tube and the exhaust products were measured with a gas chromatograph. The mT-FFC showed a promising peak power density of 460 mW cm^{−2} and the potential for high fuel utilization, which exceeded 50% at an equivalence ratio of 4.6. The present micro flow reactor with controlled temperature profile was demonstrated as a possible non-catalytic fuel reformer for hydrocarbons to syngas. Syngas formation was shown to be temperature dependent which makes variations of the wall temperature, flow rate and equivalence ratio important. More work is needed to optimize the exhaust composition to increase the mT-FFC performance and long-term operation. Peak syngas concentrations achieved in this study are still well below chemical equilibrium predictions which warrants further investigation. Soot formation in the micro flow reactor was shown to decrease drastically between a wall temperature of 900 and 950 °C with propane/air flames. No soot formation at an equivalence ratio of 5.5 was demonstrated for wall temperatures between 750 and 900 °C.

Acknowledgements

This material is based upon work supported by an agreement with Syracuse University awarded by its Syracuse Center of Excellence for Environmental and Energy Systems with funding under prime award number DE-EE0006031 from the U.S. Department of Energy and matching funding under award number 53367 from the New York State Energy Research and Development Authority, under NYSERDA contract 61736 and NEXUS-NY. This material is also based upon work supported by the National Science Foundation Graduate Research Fellowship Program under Grant No. 1746928 and the National Science Foundation Graduate Research Opportunities Worldwide. Part of the work was carried out under the Collaborative Research Project of the Institute of Fluid Science, Tohoku University, supported by JSPS KAKENHI Grant Number JP16H06068 and the corresponding author was a JSPS International Research Fellow.

Appendix A. Supplementary data

Supplementary data to this article can be found online at <https://doi.org/10.1016/j.jpowsour.2018.12.043>.

References

- [1] M. Horiuchi, S. Suganuma, M. Watanabe, Electrochemical power generation directly from combustion flame of gases, liquids, and solids, *J. Electrochem. Soc.* 151 (2004) A1402, <https://doi.org/10.1149/1.1778168>.
- [2] H. Kronmayer, D. Barzan, M. Horiuchi, S. Suganuma, Y. Tokutake, C. Schulz, W.G. Bessler, A direct-flame solid oxide fuel cell (DFFC) operated on methane, propane, and butane, *J. Power Sources* 166 (2007) 120–126, <https://doi.org/10.1016/j.jpowsour.2006.12.074>.
- [3] K. Wang, R. Ran, Y. Hao, Z. Shao, W. Jin, N. Xu, A high-performance no-chamber fuel cell operated on ethanol flame, *J. Power Sources* 177 (2008) 33–39, <https://doi.org/10.1016/j.jpowsour.2007.11.004>.
- [4] K. Wang, P. Zeng, J. Ahn, High performance direct flame fuel cell using a propane flame, *Proc. Combust. Inst.* 33 (2011) 3431–3437, <https://doi.org/10.1016/j.proci.2010.07.047>.
- [5] Y. Wang, Y. Shi, X. Yu, N. Cai, Thermal shock resistance and failure probability analysis on solid oxide electrolyte direct flame fuel cells, *J. Power Sources* 255 (2014) 377–386, <https://doi.org/10.1016/j.jpowsour.2014.01.035>.
- [6] Y. Wang, Y. Shi, X. Yu, N. Cai, J. Qian, S. Wang, Experimental characterization of a direct methane flame solid oxide fuel cell power generation unit, *J. Electrochem. Soc.* 161 (2014) F1348–F1353, <https://doi.org/10.1149/2.0381414jes>.
- [7] K. Wang, R.J. Milcarek, P. Zeng, J. Ahn, Flame-assisted fuel cells running methane, *Int. J. Hydrogen Energy* 40 (2015) 4659–4665, <https://doi.org/10.1016/j.ijhydene.2015.01.128>.
- [8] Y. Wang, H. Zeng, Y. Shi, T. Cao, N. Cai, X. Ye, S. Wang, Power and heat co-generation by micro-tubular flame fuel cell on a porous media burner, *Energy* 109 (2016) 117–123, <https://doi.org/10.1016/j.energy.2016.04.095>.
- [9] Y. Wang, H. Zeng, T. Cao, Y. Shi, N. Cai, X. Ye, S. Wang, Start-up and operation characteristics of a flame fuel cell unit, *Appl. Energy* 178 (2016) 415–421, <https://doi.org/10.1016/j.apenergy.2016.06.067>.
- [10] M.C. Tucker, A.S. Ying, Metal-supported solid oxide fuel cells operated in direct-flame configuration, *Int. J. Hydrogen Energy* 42 (2017) 24426–24434, <https://doi.org/10.1016/j.ijhydene.2017.07.224>.
- [11] R.J. Milcarek, K. Wang, M.J. Garrett, J. Ahn, Performance investigation of dual layer yttria-stabilized zirconia-samarium-doped ceria electrolyte for intermediate temperature solid oxide fuel cells, *J. Electrochem. Energy Convers. Storage* 13 (2016) 011002, <https://doi.org/10.1115/1.4032708>.
- [12] R.J. Milcarek, K. Wang, R.L. Falkenstein-Smith, J. Ahn, Performance variation with SDC buffer layer thickness, *Int. J. Hydrogen Energy* 41 (2016) 9500–9506, <https://doi.org/10.1016/j.ijhydene.2016.04.113>.
- [13] R.J. Milcarek, K. Wang, R.L. Falkenstein-Smith, J. Ahn, Micro-tubular flame-assisted fuel cells for micro-combined heat and power systems, *J. Power Sources* 306 (2016) 148–151, <https://doi.org/10.1016/j.jpowsour.2015.12.018>.
- [14] R.J. Milcarek, M.J. Garrett, A. Baskaran, J. Ahn, Combustion characterization and model fuel development for micro-tubular flame-assisted fuel cells, *J. Vis. Exp.* (2016) e54638, <https://doi.org/10.3791/54638>.
- [15] R.J. Milcarek, M.J. Garrett, K. Wang, J. Ahn, Micro-tubular flame-assisted fuel cells running methane, *Int. J. Hydrogen Energy* 41 (2016) 20670–20679, <https://doi.org/10.1016/j.ijhydene.2016.08.155>.
- [16] R.J. Milcarek, M.J. Garrett, J. Ahn, Micro-tubular flame-assisted fuel cell stacks, *Int. J. Hydrogen Energy* 41 (2016) 21489–21496, <https://doi.org/10.1016/j.ijhydene.2016.09.005>.
- [17] R.J. Milcarek, J. Ahn, Rich-burn, flame-assisted fuel cell, quick-mix, lean-burn (RFQL) combustor and power generation, *J. Power Sources* 381 (2018) 18–25, <https://doi.org/10.1016/j.jpowsour.2018.02.006>.
- [18] R.J. Milcarek, M.J. Garrett, T.S. Welles, J. Ahn, Performance investigation of a micro-tubular flame-assisted fuel cell stack with 3,000 rapid thermal cycles, *J. Power Sources* 394 (2018) 86–93, <https://doi.org/10.1016/j.jpowsour.2018.05.060>.
- [19] S.R. Turns, *An Introduction to Combustion: Concepts and Applications*, second ed., McGraw-Hill, New York, 2000.
- [20] R.J. Milcarek, M.J. Garrett, J. Ahn, Micro-tubular flame-assisted fuel cells, *J. Fluid Sci. Technol.* 12 (2017), <https://doi.org/10.1299/jfst.2017jfst0021>.
- [21] K. Kendall, C.M. Finnerty, J.C. Austin, T. Alston, Ceramic fuel cells to replace metal burners, *J. Mater. Sci.* 36 (2001) 1119–1124, <https://doi.org/10.1023/A:1004869522984>.
- [22] K. Kendall, M. Kendall, *High-temperature Solid Oxide Fuel Cells for the 21st Century: Fundamentals, Design and Applications*, Academic Press, New York, 2016.
- [23] K. Kendall, Catalysts for butane reforming in zirconia fuel cells, *Platin. Met. Rev.* 42 (1998) 164–167.
- [24] M.K. Drayton, A.V. Saveliev, L.A. Kennedy, A.A. Fridman, Y.-E. Li, Syngas production using superadiabatic combustion of ultra-rich methane-air mixtures, *Proc. Combust. Inst.* (1998) 1361–1367, <https://doi.org/10.1016/j.ijhydene.2008.10.085>.
- [25] Y. Ju, C. Cadou, K. Maruta, *Microscale Combustion and Power Generation*, Momentum Press, New York, 2015.
- [26] I. Schoegl, J.L. Ellzey, Superadiabatic combustion in conducting tubes and heat exchangers of finite length, *Combust. Flame* 151 (2007) 142–159, <https://doi.org/10.1016/j.combustflame.2007.01.009>.
- [27] K. Maruta, T. Kataoka, N. Il Kim, S. Minaev, R. Fursenko, Characteristics of combustion in a narrow channel with a temperature gradient, *Proc. Combust. Inst.* 30 (2005) 2429–2436, <https://doi.org/10.1016/j.proci.2004.08.245>.
- [28] T. Okuno, H. Nakamura, T. Tezuka, S. Hasegawa, K. Maruta, Ultra-lean combustion characteristics of premixed methane flames in a micro flow reactor with a controlled temperature profile, *Proc. Combust. Inst.* 36 (2017) 4227–4233, <https://doi.org/10.1016/j.proci.2016.06.137>.
- [29] I. Schoegl, J.L. Ellzey, A mesoscale fuel reformer to produce syngas in portable power systems, *Proc. Combust. Inst.* 32 (2009) 3223–3230, <https://doi.org/10.1016/j.proci.2008.06.079>.
- [30] L.A. Kennedy, J.P. Bingue, A.V. Saveliev, A.A. Fridman, S.I. Foutko, Chemical structures of methane-air filtration combustion waves for fuel-lean and fuel-rich conditions, *Proc. Combust. Inst.* 28 (2000) 1431–1438, [https://doi.org/10.1016/S0082-0784\(00\)80359-8](https://doi.org/10.1016/S0082-0784(00)80359-8).
- [31] R.S. Dhamrat, J.L. Ellzey, Numerical and experimental study of the conversion of methane to hydrogen in a porous media reactor, *Combust. Flame* 144 (2006) 698–709, <https://doi.org/10.1016/j.combustflame.2005.08.038>.
- [32] J. Ahn, C. Eastwood, L. Sitzki, P.D. Ronney, Gas-phase and catalytic combustion in heat-recirculating burners, *Proc. Combust. Inst.* 30 (2005) 2463–2472, <https://doi.org/10.1016/j.proci.2004.08.265>.
- [33] N. Kim, S. Kato, T. Kataoka, T. Yokomori, S. Maruyama, T. Fujimori, K. Maruta, Flame stabilization and emission of small swiss-roll combustors as heaters, *Combust. Flame* 141 (2005) 229–240, <https://doi.org/10.1016/j.combustflame.2005.01.006>.
- [34] F.J. Weinberg, T.G. Bartleet, F.B. Carleton, P. Rimbotti, J.H. Brophy, R.P. Manning, Partial oxidation of fuel-rich mixtures in a spouted bed combustor, *Combust. Flame* 72 (1988) 235–239, [https://doi.org/10.1016/0010-2180\(88\)90124-1](https://doi.org/10.1016/0010-2180(88)90124-1).
- [35] F. Takahashi, I. Glassman, Sooting correlations for premixed flames, *Combust. Sci. Technol.* 37 (1984) 1–19, <https://doi.org/10.1080/00102208408923743>.
- [36] A.K. Dubey, T. Tezuka, S. Hasegawa, H. Nakamura, K. Maruta, Study on sooting behavior of premixed C1 – C4 n-alkanes/air flames using a micro flow reactor with a controlled temperature profile, *Combust. Flame* 174 (2016) 100–110, <https://doi.org/10.1016/j.combustflame.2016.09.007>.
- [37] H. Nakamura, S. Suzuki, T. Tezuka, S. Hasegawa, K. Maruta, Sooting limits and PAH formation of n-hexadecane and 2,2,4,4,6,8,8-heptamethylnonane in a micro flow reactor with a controlled temperature profile, *Proc. Combust. Inst.* 35 (2015) 3397–3404, <https://doi.org/10.1016/j.proci.2014.05.148>.
- [38] K. Kendall, Progress in microtubular solid oxide fuel cells, *Int. J. Appl. Ceram. Technol.* 7 (2010) 1–9, <https://doi.org/10.1111/j.1744-7402.2008.02350.x>.
- [39] A. Di Stazio, C. Chauveau, G. Dayma, P. Dagaut, Pulsating combustion of ethylene in micro-channels with controlled temperature gradient, 26th ICDERS, 2017, pp. 1–7.
- [40] J. Warnatz, The mechanism of high temperature combustion of propane and butane, *Combust. Sci. Technol.* 34 (1983) 177–200, <https://doi.org/10.1080/00102208308923692>.
- [41] D.C. Walther, J. Ahn, Advances and challenges in the development of power-generation systems at small scales, *Prog. Energy Combust. Sci.* 37 (2011) 583–610, <https://doi.org/10.1016/j.pecs.2010.12.002>.
- [42] Y. Ju, K. Maruta, Microscale combustion: technology development and fundamental research, *Prog. Energy Combust. Sci.* 37 (2011) 669–715, <https://doi.org/10.1016/j.pecs.2011.03.001>.
- [43] Y. Matsuzaki, I. Yasuda, Electrochemical oxidation of H₂ and CO in a H₂-H₂O-CO-CO₂ system at the interface of a Ni-YSZ cermet electrode and YSZ electrolyte, *J. Electrochem. Soc.* 147 (2000) 1630, <https://doi.org/10.1149/1.1393409>.
- [44] R.J. Gorte, S. Park, J.M. Vohs, Direct oxidation of hydrocarbons in a solid-oxide fuel cell, *Nature* 404 (2000) 265–267, <https://doi.org/10.1038/35005040>.
- [45] S. Park, R. Craciun, J.M. Vohs, R.J. Gorte, Direct oxidation of hydrocarbons in a solid oxide fuel cell. I. Methane oxidation, *J. Electrochem. Soc.* 146 (1999) 3603–3605.
- [46] A. Aarva, M. Noponen, J. Kiviahio, Effect of ethene impurity on performance of solid oxide fuel cell, *ECS Trans. ECS*, 2007, pp. 1653–1659, <https://doi.org/10.1149/1.2729274>.

Glossary

- DFFC: Direct flame fuel cell
 F: Faraday constant
 FFC: Flame-assisted fuel cell
 FREE: Flame with repetitive extinction and ignition
 GC: Gas chromatograph
 i: Current
 LSCF: Lanthanum strontium cobalt ferrite
 mT-FFC: micro-tubular flame-assisted fuel cell
 mT-SOFC: micro-tubular solid oxide fuel cell
 n_{fuel} : Molar flow rate of fuel
 n_{air} : Molar flow rate of air
 n_{fuel}^S : Molar flow rate of fuel for stoichiometric reaction
 n_{air}^S : Molar flow rate of air for stoichiometric reaction
 SDC: Samaria-doped Ceria
 SOFC: Solid oxide fuel cell
 V^M : Molar volume at standard conditions
 V_{fuel} : Flowrate of propane
 YSZ: Yttria stabilized zirconia, (Y₂O₃)_{0.08}(ZrO₂)_{0.92}
 Φ : Equivalence ratio
 $\epsilon_{F.U.}$: Fuel utilization